

High-Temperature Photoluminescence in Colloidal “Quasi” 2D Materials

Alexey Y. Koposov,^{*,†,||} Bryan T. Spann,[‡] Alina Bruma,[§] Paul Schuele,[†] Kris Bertness,[‡] and Albert Davydov[§]

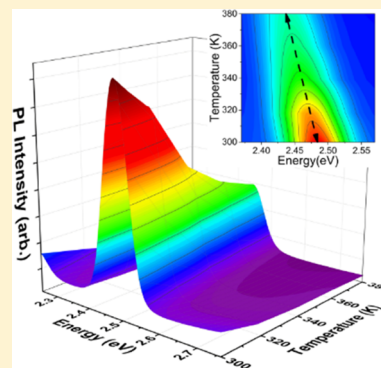
[†]Materials and Devices Applications Laboratory, Sharp Laboratories of America, Inc., 5750 NW Pacific Rim Blvd., Camas, Washington 98607, United States

[‡]Applied Physics Division, National Institute of Standards and Technology, 325 Broadway, Boulder, Colorado 80305, United States

[§]Material Science and Engineering Division, Material Measurement Laboratory, National Institute of Standards and Technology, 100 Bureau Drive, Gaithersburg, Maryland 20899, United States

S Supporting Information

ABSTRACT: The recent development of quasi-two-dimensional (2D) semiconducting nanomaterials [nanoplatelets (NPLs)] prepared through solution-based chemistry has attracted significant attention in the field of color conversion materials. Herein, we demonstrate the efficient high-temperature photoluminescence of the as-prepared cadmium telluride NPLs from 300 to 500 K with visually observable emission at temperatures as high as 500 K. Indeed, the thermal-emission quenching of the as-prepared NPLs in solution was found to be not only reversible following thermal cycling up to 475 K, but also comparable to more chemically complex core/shell nanostructures. To the best of our knowledge, this is the first example of the as-synthesized colloidal nanoparticles capable of high-temperature photoluminescence. This discovery highlights previously unexplored emission properties of NPLs that have the potential to be utilized for the efficient design of high-quality light emitters.



INTRODUCTION

The rational design of highly efficient color-converting nanomaterials is essential for modern lighting and display technologies with low energy consumption. The demand for high light quality and efficiency motivated the development of quantum-confined materials, wherein semiconductor quantum dots (QDs) likely represent the most appropriate class of materials for color conversion applications.¹ However, within one of the most efficient designs in high-quality light-emitting diode (LED) lighting, the color-converting material is subjected to operating temperatures around 390–425 K,² including those ranges at which the performance of the as-prepared QDs deteriorate rapidly because of “thermal quenching”, which can be partially mitigated.^{3–5}

The recently discovered semiconducting nanoplatelets (NPLs), which can be described as quasi-two-dimensional (2D) materials, may be accessed through analogous chemistries and techniques for preparing QDs.^{6–8} The synthetic pathway that utilizes cadmium acetate or propionate facilitates lamellar nanoparticle growth, allowing the formation of quasi-2D, sheet-type nanostructures. The electronic band structure of NPLs is controlled by both the thickness and the chemical nature of the materials. Analogous to QDs and other nanomaterials prepared through colloidal chemistry, NPLs have a shell of surface-passivating ligands which assist in the controlled growth, prevent particle aggregation, and, to some extent, tailor the band gap of the material.⁹ The synthesis of various examples

with different chemical compositions, such as CdS, CdSe, cadmium telluride (CdTe), and PbSe, as well as cadmium mixed sulfide-selenide, has been demonstrated in the literature.^{10–12} Within the context of color-conversion applications, cadmium-based materials are of particular interest because of a band gap that permits electronic transitions in the visible region of the electromagnetic spectrum. The extremely narrow emission lines and the versatile solution-based synthetic protocols for such nanomaterials make them attractive for color-converting applications; although, the toxicity of cadmium-based materials is potentially problematic for a widespread adoption. Although NPL's emission properties have been investigated at low temperatures,^{13,14} its performance at elevated temperatures, such as the operating temperature of LEDs (390–425 K), demonstrates industrial potential for these materials as color converters. To the best of our knowledge, this is the first study that demonstrates retention of emission properties for the as-prepared, uncoated semiconducting NPLs at elevated temperatures performed entirely in solution, wherein the nanoparticles are prone to ripening and/or ligand dissociation, either of which would negatively impact emission properties.

Received: October 26, 2017

Revised: February 11, 2018

Published: February 13, 2018

RESULTS AND DISCUSSION

The CdTe NPLs were prepared by a continuous injection method using a previously reported procedure.¹⁵ The detailed procedure for the preparation of the NPLs is described in the [Supporting Information](#). The prepared NPLs consist of either six or seven layers of CdTe (often also reported as an integer number of CdTe layers or total number of atomic layers¹⁶). Although the adopted synthetic procedure was originally reported for the preparation of seven layers, in our case, such synthesis often resulted in nanoparticles with an emission maximum at 501 nm, which corresponds to six layers of CdTe, based on the assignment previously reported.⁸ A typical synthesis yielded particles with the optical signatures in absorption and emission spectra common for these quasi-2D materials ([Figure S1](#)). [Figure 1A](#) presents a low-magnification

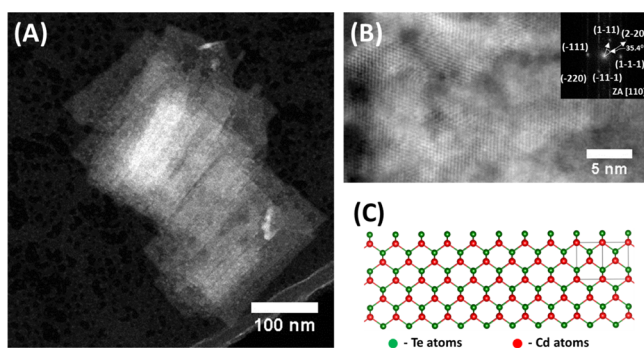


Figure 1. (A) Low-magnification HAADF-STEM image of CdTe platelets dispersed onto the surface of amorphous carbon; (B) high-magnification HAADF-STEM image of CdTe platelets together with the FFT pattern in the inset; (C) structural model of the CdTe platelets in $[110]$ projection. Green atoms: Te and red atoms: Cd.

high-angle annular dark-field scanning transmission electron microscopy (HAADF-STEM) image of the CdTe platelets dispersed onto the surface of the grid (also shown as in the scanning electron microscopy (SEM) image in [Figure S1](#)). Our analysis confirms that most platelets exhibit rectangular morphologies with dimensions of $\sim 50 \times 200$ nm. [Figure 1B](#) shows a high-magnification HAADF-STEM image of a typical CdTe platelet in $[110]$ zone axis, as evident from the fast Fourier transform (FFT) analysis, as shown in the inset, and exhibits a nonuniform surface yet with a clearly distinguishable atomic arrangement. [Figure 1C](#) shows a planar structural model of such a platelet in $[110]$ projection (the three-dimensional model is shown in [Figure S2](#)). The NPLs have a zinc blende, $F\bar{4}3m$ structure, with the basal surface of (220) ([Figure 1C](#)) consistent with the X-ray diffraction analysis ([Supporting Information](#), [Figure S3](#)). The energy-dispersive spectrometry (EDS) analysis determined a slight Cd excess in NPLs compared to stoichiometric composition which might be because of a metal-enriched surface. Following the synthesis, aggregation of the NPLs occurred within 2–3 weeks (depicted on SEM image on [Figure S4](#)) and consequently resulted in a loss of emission properties, which has been previously observed.¹⁷ Therefore, all studies reported in the present communication were performed with freshly prepared samples. To suppress aggregation of the particles, all measurements were conducted in the presence of an excess oleic acid—a common ligand for NPLs.¹⁸

The typical results of the steady-state emission measurements at variable temperatures are shown in [Figure 2](#).

Remarkably, the emission of the nanoparticles is not only detectable, but clearly visible at temperatures above 493 K, which is substantially higher than the desired operating temperature of typical color conversion materials (350–425 K, depending on the device architecture), which makes the quasi-2D NPLs a one-of-a-kind candidate for such applications. To ensure that such astonishing emission stability originated from the NPLs themselves, we performed extensive purification of the NPLs through conventional precipitation and redispersion methodologies, which are commonly utilized for the purification of colloidal prepared nanostructures. Upon purification and redispersion in 1-octadecene (ODE), the NPLs still exhibit visible, high-temperature photoluminescence, which directly confirms that such an effect is due to the intrinsic properties of the material rather than the formation of other emissive species over the course of the reaction. It is worth noting that the emission of purified NPLs is still visible by the naked eye at temperatures exceeding 473 K. At the same time, the purified NPLs substantially lose their colloidal stability because of aggregation, which significantly limits the measurement time frame. Therefore, the measurements presented in this communication were conducted using a reaction mixture diluted with ODE including an additional surfactant (oleic acid). High-temperature photoluminescence could even be observed during the synthesis of the NPLs—within approximately 5 min after starting the addition of the tellurium precursor; the reaction flask could be illuminated by a UV lamp (320 nm wavelength) to reveal a clearly visible emission, as shown in the inset of the [Figure 2A](#). Not surprisingly, as the sample temperature rises, we observed a drop in the emission intensity, with partial recovery at 423 K. Such a recovery is due to the formation of gas bubbles (originating from nitrogen dissolved in a solvent), which results in the NPL concentration variation that complicates an absolute assessment of the emission intensities at temperatures above 423 K. Therefore, qualitative analysis of the emission changes has been performed only in the range of 300–381 K ([Figure 2B](#)). The changes in photoluminescence intensities were also accompanied by red-shifting the emission maxima ([Figure 2C](#)). The shift as a function of temperature is shown in [Figure 2D](#), which demonstrated the consistency of shifts observed for the NPLs with a Varshni-like dependence of the band gap change, similar to previously reported CdTe QDs^{19,20} (further details are shown in the [Supporting Information](#)). Similar shifts measured at low temperatures have been previously observed on CdSe NPLs.⁸

The changes in emission properties occurring at elevated temperatures were found to be reversible—upon cooling the mixture from 476 K to room temperature, the original emission spectrum was restored. Similar behavior has been previously observed only for more complex core/shell heterostructures, such as CdTe/CdSe,³ InP/ZnS,⁵ or Si nanocrystals with covalently bound ligands.²¹ The irreversible thermal quenching at elevated temperatures is generally attributed to changes in surface chemistry of the semiconducting nanoparticles. For instance, lead sulfide nanoparticles in solution undergo a “refocusing” process at temperatures close to 375 K.²² More conventional CdSe and CdTe QDs are also known to permanently lose their emission properties after exposure to heating cycles.³ Generally, to mitigate surface reconstruction and eliminate irreversible structural changes and resultant reduced emission properties for QDs, growth of the additional shells is required, which provides surface tolerance to the

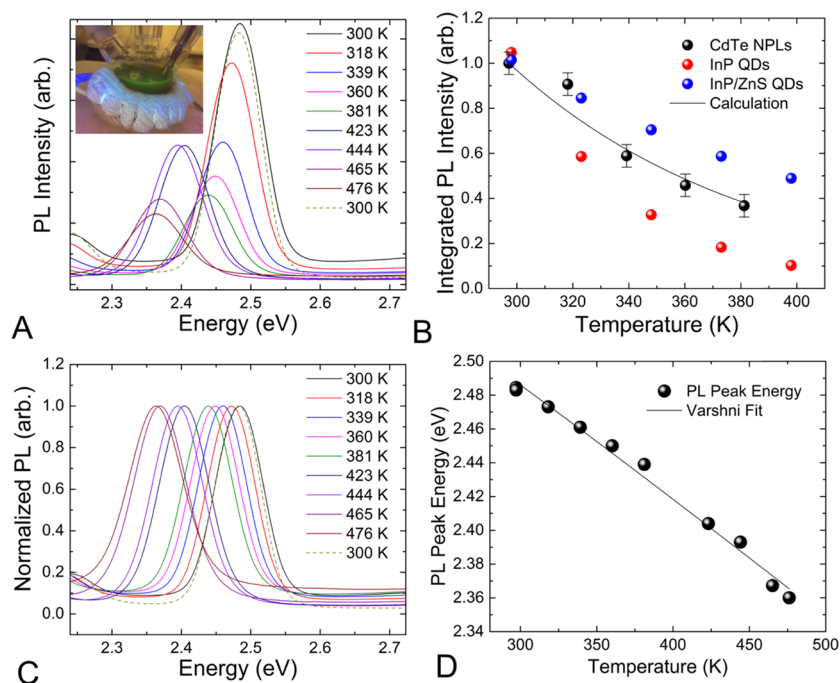


Figure 2. (A) Emission changes at elevated temperatures measured on stirred samples with an excitation wavelength of 266 nm; the inset shows the image of the reaction flask exposed to a UV lamp during the later stages of synthesis at a temperature of 498 K, demonstrating visible photoluminescence; (B) normalized integrated emission within the range 300–381 K in comparison with the calculated values for films of InP and InP/ZnS using $I(T) = Ae^{[-(T-300)/\zeta]}$ using ζ parameters reported in ref 5; (C) normalized emission in the temperature range 300–476 K; (D) changes in the energy of the emission peak maximum as a function of the temperature. Note: dashed lines in (A,C) represent spectra taken after the sample has cooled down.

thermally induced restructuring.²⁰ However, in case of NPLs, the absence of irreversible quenching eliminates a critical factor that would otherwise limit the practical application of these nanomaterials. Moreover, the changes of the emission properties are also attributed to the changes in the nature of interactions between the nanostructures and surface ligands—an effect which has been observed in CdSe nanocrystals³ and in recently reported CsPbI₃ nanocrystals, which completely lose their emitting properties at temperatures around 420 K.²³ As expected, the emission lines are characterized by a small broadening at elevated temperatures because of the changes in phonon–exciton coupling, with increased full half width maximum by approximately 10 meV with a temperature change from 300 to 444 K, which is close to the values observed on more complex dot-in-rod nanostructures.²⁴

Noteworthy, the changes of the integrated PL intensity at 381 K (a common exposure temperature for color-converting materials in LEDs) demonstrated a drop to approximately one-third of the original emission intensity. The temperature dependence of the integrated emission allows calculation of the temperature sensitivity parameter (ζ)—a measure of the temperature effect on the emission intensity, whereby higher values of ζ correspond to lower quenching of the emission intensity with elevation of temperature. That value of ζ is calculated from the decay of the emission as a function of temperature approximated with $I(T) = Ae^{[-(T-300)/\zeta]}$, where $I(T)$ is the emission intensity at a given temperature, $A = 1$, for the data normalized to the value at 300 K.⁵ For the NPL samples utilized in the present work, values of ζ were calculated to be 90–100 depending on the sample. We believe that the discrepancy in results originates from the solution-based measurements, which at elevated temperatures, was accom-

panied by the formation of gas bubbles arising from the nitrogen dissolved in the solvent. Such ζ values were reported for InP QDs. Importantly, the values calculated for NPL samples were substantially above the value obtained for InP cores (43) and close to the value obtained for more chemically complex nanocrystals treated with inorganic ligands (87 and 109).⁵ However, we believe that the comparison of these measurements may not be completely appropriate since InP QDs were measured in a film, whereas measurements presented in this work were carried out in a solution, where the ligands and surface atoms are more labile and may exert an influence on the emission quenching process.

Herein, we employed time-resolved photoluminescence measurements, which often provide critical insights into excited-state recombination mechanisms (Figure 3A). For instance, this technique allows one to distinguish between two types of quenching mechanisms described in the literature—dynamic and static. Dynamic quenching, which originates from a thermally activated trapping mechanism, results in decreasing emission lifetimes. Static quenching is related to a decrease in the number of emitting particles, that is, an increase in the fraction of “dark” particles, which is substantiated by the decrease in amplitude of the emission decay curve. Within the present system, we did not observe changes of the emission lifetimes, whereas the decreases in amplitude with temperature elevation were indicative of static quenching (Figure 3A,B). The measurements of time-resolved emission revealed biexponential decay with weighted average lifetimes ranging from approximately 300 to 420 ps, which were calculated using standard techniques (see the Supporting Information for more details).²⁵ Similar behavior for NPLs has been reported previously, where two components in the

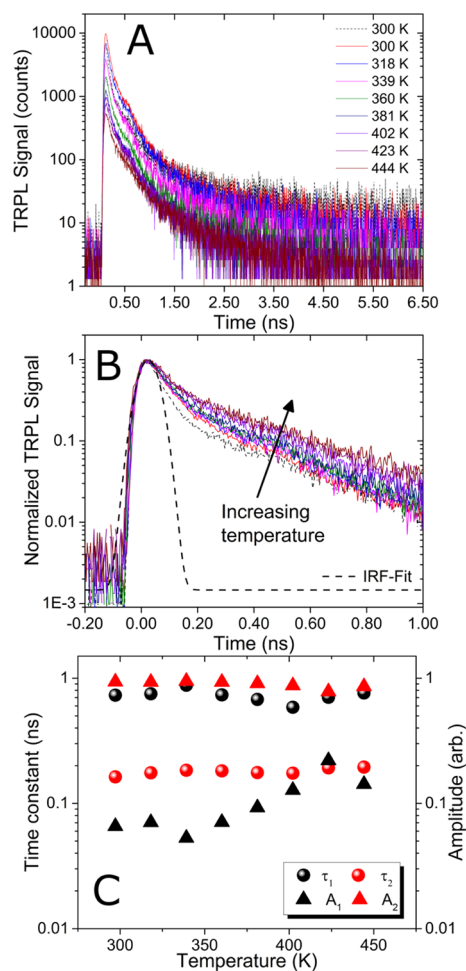


Figure 3. (A) Time-resolved emission changes at elevated temperatures monitored at emission peak maximum wavelength for each temperature point to account for band gap change; (B) normalized emission decay curves; and (C) evolution of bright and dark exciton lifetimes as a function of temperature.

emission decay have been attributed to bright and dark exciton states.^{13,14} However, at temperatures described in the present work, the bright and dark states should be in a thermodynamic equilibrium. The biexponential behavior of the PL dynamics could be explained by the presence of the NPLs with and without the quenching site.²⁶ The fast component (around 180 ps) corresponds to the quenching of the exciton, whereas the longer component (varying from about 600 to almost 900 ps depending on the temperature) corresponds to the decay of excitons in NPLs without the quenching site. It is worth noting that in our case, the lifetime of the exciton of NPLs with a quenching site does not change at elevated temperatures, whereas no appearance of additional decay pathways were observed. Therefore, we can assume that elevated temperatures do not introduce alternative nonradiative or trap-related relaxation pathways with the exception of ligand loss. The thermally initiated ligand losses because of induced ligand lability should result in the formation of positive charge on the NPL surface, which would serve as temporary trap states until the room temperature equilibrium is restored.²⁷ We believe that such trapping may occur at high rate and thus is not observed in the time-resolved measurements presented here, whereas the short lifetime component could be clearly assigned to the internally quenched emission. The ligand loss at the elevated

temperature was indirectly confirmed by heating the purified sample in pure ODE with subsequent cooling, which resulted in the immediate aggregation of NPLs evidenced by precipitation.

CONCLUSIONS

In conclusion, we have investigated quasi-2D CdTe NPLs at those elevated temperatures that are common for color-converting applications. Interestingly, these materials have demonstrated substantial retention of emission properties following high-temperature cycling. Moreover, we anticipate that with the appropriate choice of matrix material, the temperature quenching of NPLs could be additionally minimized. Our preliminary results also indicate that similar effects could be observed not only for CdTe NPLs of various thicknesses, but also for NPLs with different chemical compositions, such as CdSe NPLs, which would be reflected in a follow-up publication. Such results have important implications on the future development of nanostructured materials utilized in optical technologies. Therefore, the presented research not only elucidates important fundamental phenomena, but also exemplifies the promising potential for NPLs as color-converting materials in modern LEDs.

ASSOCIATED CONTENT

Supporting Information

The Supporting Information is available free of charge on the ACS Publications website at DOI: 10.1021/acs.jpcc.7b10615.

Synthetic and measurements details, additional structural characterization, and optical spectra of nanostructures (PDF)

AUTHOR INFORMATION

Corresponding Author

*E-mail: kopo0003@gmail.com, Alexey.Koposov@ife.no.

ORCID

Alexey Y. Koposov: 0000-0001-5898-3204

Albert Davydov: 0000-0003-4512-2311

Present Address

^{||}Battery Technology Department, Institute for Energy Technology (IFE), Instituttveien 18, NO-2007 Kjeller, Norway.

Author Contributions

The manuscript was written through contributions from all authors. All authors have given approval to the final version of the manuscript.

Notes

The authors declare no competing financial interest.

ACKNOWLEDGMENTS

A.Y.K. and P.S. acknowledge the support of “Sharp Dream Technology” funding provided by Corporate Research and Development Division of SHARP Corporation. B.T.S. acknowledges the support of the National Research Council for administering his postdoctoral fellowship.

ABBREVIATIONS

QD, quantum dot; NPL, nanoplatelet; LED, light-emitting diode; HAADF-STEM, high-angle annular dark-field scanning transmission electron microscopy; UV, ultraviolet; FWHM, full half width maximum; ODE, 1-octadecene

REFERENCES

- (1) Coltrin, M. E.; Armstrong, A. M.; Brener, I.; Chow, W. W.; Crawford, M. H.; Fischer, A. J.; Kelley, D. F.; Koleske, D. D.; Lauhon, L. J.; Martin, J. E.; et al. Energy Frontier Research Center for Solid-State Lighting Science: Exploring New Materials Architectures and Light Emission Phenomena. *J. Phys. Chem. C* **2014**, *118*, 13330–13345.
- (2) Wang, K.; Sun, X. W. *Quantum-Dot and Quantum-Rod Displays—the Next Big Wave*; SID Information Display, 2016; Vol. 32, pp 6–14.
- (3) Zhao, Y.; Riemersma, C.; Pietra, F.; Koole, R.; de Mello Donegá, C.; Meijerink, A. High-Temperature Luminescence Quenching of Colloidal Quantum Dots. *ACS Nano* **2012**, *6*, 9058–9067.
- (4) Cai, X.; Martin, J. E.; Shea-Rohwer, L. E.; Gong, F.; Kelley, D. F. Thermal Quenching Mechanisms in II–VI Semiconductor Nanocrystals. *J. Phys. Chem. C* **2013**, *117*, 7902–7913.
- (5) Rowland, C. E.; Liu, W.; Hannah, D. C.; Chan, M. K. Y.; Talapin, D. V.; Schaller, R. D. Thermal Stability of Colloidal InP Nanocrystals: Small Inorganic Ligands Boost High-Temperature Photoluminescence. *ACS Nano* **2014**, *8*, 977–985.
- (6) Nasilowski, M.; Mahler, B.; Lhuillier, E.; Ithurria, S.; Dubertret, B. Two-Dimensional Colloidal Nanocrystals. *Chem. Rev.* **2016**, *116*, 10934–10982.
- (7) Ithurria, S.; Dubertret, B. Quasi 2D Colloidal CdSe Platelets with Thicknesses Controlled at the Atomic Level. *J. Am. Chem. Soc.* **2008**, *130*, 16504–16505.
- (8) Ithurria, S.; Tessier, M. D.; Mahler, B.; Lobo, R. P. S. M.; Dubertret, B.; Efros, A. L. Colloidal nanoplatelets with two-dimensional electronic structure. *Nat. Mater.* **2011**, *10*, 936–941.
- (9) Szemjonov, A.; Pauporté, T.; Ithurria, S.; Lequeux, N.; Dubertret, B.; Ciofini, I.; Labat, F. Ligand-stabilized CdSe nanoplatelet hybrid structures with tailored geometric and electronic properties. New insights from theory. *RSC Adv.* **2014**, *4*, 55980–55989.
- (10) Koh, W.-k.; Dandu, N. K.; Fidler, A. F.; Klimov, V. I.; Pietryga, J. M.; Kilina, S. V. Thickness-Controlled Quasi-Two-Dimensional Colloidal PbSe Nanoplatelets. *J. Am. Chem. Soc.* **2017**, *139*, 2152–2155.
- (11) Schlenskaya, N. N.; Yao, Y.; Mano, T.; Kuroda, T.; Garshev, A. V.; Kozlovskii, V. F.; Gaskov, A. M.; Vasiliev, R. B.; Sakoda, K. Scroll-like Alloyed CdS_xSe_{1-x} Nanoplatelets: Facile Synthesis and Detailed Analysis of Tunable Optical Properties. *Chem. Mater.* **2017**, *29*, 579–586.
- (12) Fan, F.; Kanjanaboos, P.; Saravanapavanantham, M.; Beauregard, E.; Ingram, G.; Yassitepe, E.; Adachi, M. M.; Voznyy, O.; Johnston, A. K.; Walters, G.; et al. Colloidal CdSe_{1-x}S_x Nanoplatelets with Narrow and Continuously-Tunable Electroluminescence. *Nano Lett.* **2015**, *15*, 4611–4615.
- (13) Biadala, L.; Liu, F.; Tessier, M. D.; Yakovlev, D. R.; Dubertret, B.; Bayer, M. Recombination Dynamics of Band Edge Excitons in Quasi-Two-Dimensional CdSe Nanoplatelets. *Nano Lett.* **2014**, *14*, 1134–1139.
- (14) Scott, R.; Kickhöfel, S.; Schoeps, O.; Antanovich, A.; Prudnikau, A.; Chuvilin, A.; Woggon, U.; Artemyev, M.; Achtstein, A. W. Temperature dependent radiative and non-radiative recombination dynamics in CdSe–CdTe and CdTe–CdSe type II hetero nanoplatelets. *Phys. Chem. Chem. Phys.* **2016**, *18*, 3197–3203.
- (15) Pedetti, S.; Nadal, B.; Lhuillier, E.; Mahler, B.; Bouet, C.; Abécassis, B.; Xu, X.; Dubertret, B. Optimized Synthesis of CdTe Nanoplatelets and Photoresponse of CdTe Nanoplatelets Films. *Chem. Mater.* **2013**, *25*, 2455–2462.
- (16) Szemjonov, A.; Pauporté, T.; Ithurria, S.; Lequeux, N.; Dubertret, B.; Ciofini, I.; Labat, F. Ligand-stabilized CdSe nanoplatelet hybrid structures with tailored geometric and electronic properties. New insights from theory. *RSC Adv.* **2014**, *4*, 55980–55989.
- (17) Guzelturk, B.; Erdem, O.; Olutas, M.; Kelestemur, Y.; Demir, H. V. Stacking in Colloidal Nanoplatelets: Tuning Excitonic Properties. *ACS Nano* **2014**, *8*, 12524–12533.
- (18) She, C.; Fedin, I.; Dolzhenkov, D. S.; Demortière, A.; Schaller, R. D.; Pelton, M.; Talapin, D. V. Low-Threshold Stimulated Emission Using Colloidal Quantum Wells. *Nano Lett.* **2014**, *14*, 2772–2777.
- (19) Murphy, G. P.; Zhang, X.; Bradley, A. L. Temperature-Dependent Luminescent Decay Properties of CdTe Quantum Dot Monolayers: Impact of Concentration on Carrier Trapping. *J. Phys. Chem. C* **2016**, *120*, 26490–26497.
- (20) Chin, P. T. K.; de Mello Donegá, C.; van Bavel, S. S.; Meskers, S. C. J.; Sommerdijk, N. A. J. M.; Janssen, R. A. J. Highly Luminescent CdTe/CdSe Colloidal Heteronanocrystals with Temperature-Dependent Emission Color. *J. Am. Chem. Soc.* **2007**, *129*, 14880–14886.
- (21) Rowland, C. E.; Hannah, D. C.; Demortière, A.; Yang, J.; Cook, R. E.; Prakapenka, V. B.; Kortshagen, U.; Schaller, R. D. Silicon nanocrystals at elevated temperatures: Retention of photoluminescence and diamond silicon to β -silicon carbide phase transition. *ACS Nano* **2014**, *8*, 9219–9223.
- (22) Hines, M. A.; Scholes, G. D. Colloidal PbS Nanocrystals with Size-Tunable Near-Infrared Emission: Observation of Post-Synthesis Self-Narrowing of the Particle Size Distribution. *Adv. Mater.* **2003**, *15*, 1844–1849.
- (23) Lin, C. C.; Meijerink, A.; Liu, R.-S. Critical Red Components for Next-Generation White LEDs. *J. Phys. Chem. Lett.* **2016**, *7*, 495–503.
- (24) Diroll, B. T.; Murray, C. B. High-Temperature Photoluminescence of CdSe/CdS Core/Shell Nanoheterostructures. *ACS Nano* **2014**, *8*, 6466–6474.
- (25) Spann, B. T.; Bhat, S. V.; Nian, Q.; Rickey, K. M.; Cheng, G. J.; Ruan, X.; Xu, X. Enhancing photo-induced ultrafast charge transfer across heterojunctions of CdS and laser-sintered TiO₂ nanocrystals. *Phys. Chem. Chem. Phys.* **2014**, *16*, 10669–10678.
- (26) Kunneman, L. T.; Schins, J. M.; Pedetti, S.; Heuclin, H.; Grozema, F. G.; Houtepen, A. J.; Dubertret, B.; Siebbeles, L. D. A. Nature and Decay Pathways of Photoexcited States in CdSe and CdSe/CdS Nanoplatelets. *Nano Lett.* **2014**, *14*, 7039–7045.
- (27) Zeng, Y.; Kelley, D. F. Excited Hole Photochemistry of CdSe/CdS Quantum Dots. *J. Phys. Chem. C* **2016**, *120*, 17853–17862.

High-Temperature Photoluminescence in Colloidal "Quasi" 2D Materials

Alexey Y. Koposov, ^{*,†} Bryan T. Spann,[‡] Alina Bruma,[§] Paul Schuele,[†] Kris Bertness,[‡] Albert Davydov[§]

[†] Materials and Devices Applications Laboratory, Sharp Laboratories of America, Inc., 5750 NW Pacific Rim Blvd., Camas, WA 98607

[‡] Applied Physics Division, National Institute of Standards and Technology, 325 Broadway, Boulder, CO 80305

[§] Material Science and Engineering Division, Material Measurement Laboratory, National Institute of Standards and Technology, 100 Bureau Drive, Gaithersburg, MD 20899

SUPPORTING INFORMATION

General.

All chemical manipulations were carried out under a dry nitrogen environment using conventional Schlenck-line and glove box techniques. The following chemicals: cadmium acetate dihydrate (98%), oleic acid (90%), 1-octadecene (90%), tri-n-octylphosphine (97%), and tellurium powder (99.8%) were purchased from Aldrich Chemicals and used without further purification. Additional manipulations of nanomaterials were carried out using extra-dry solvents (ethyl alcohol, toluene and hexanes), which were purchased from Acros Organics and used without additional purification. Absorbance spectra were recorded using a Perkin Elmer Lambda 950 spectrophotometer. HAADF-STEM images were collected using an FEI Titan 80-300 electron microscope operating at 300 kV, using a camera length of 100 mrad, corresponding to an inner and outer collection angle of 70 and 399 mrad respectively. The samples were prepared by placing a droplet of solution containing CdTe platelets dispersed in hexane onto an amorphous carbon TEM grid (Agar Inc.).

Synthetic methods.

Injection mixture for tri-*n*-octylphosphine telluride (TOPTe) was prepared by dissolving 5 mmol (638 mg) of tellurium in 10 mL of tri-*n*-octylphosphine telluride at 120°C. The resulting transparent mixture was further diluted with ODE to obtain a concentration of 0.03M.

15 mL of ODE, 0.15 mL of oleic acid, and 0.45 mmol (120 mg) of cadmium acetate dihydrate (ground prior to use) were loaded into the 3-neck round bottom flask equipped with a condenser and vacuum adapter, thermocouple, septum and stirring bar. The loading was performed in a nitrogen-filled glove box. The reaction vessel was removed from the glove box and connected to a Schlenk line and heating mantle. The reaction mixture was evacuated for 1 hour at 80°C then the flask was filled with nitrogen and the temperature was set to 225°C. Meanwhile, a syringe containing a mixture of 0.03 M of TOPTe in 3 mL of ODE (prepared separately in glovebox) was installed into a syringe pump. The solution was added slowly over the course of 15 minutes at 225°C. 15 minutes after completion of chalcogenide addition, the heating mantle was removed and the reaction was allowed to cool down to room temperature. Subsequently, the reaction flask was moved to the glovebox for further use. Additional purification of the nanoplatelets was carried out in a nitrogen filled glovebox using a standard technique including addition of ethanol, centrifugation and redispersion in toluene, hexane or ODE.

Measurement techniques.

Due to its high boiling point (588 K), 1-octadecene (ODE) was utilized as a primary solvent to prevent solvent evaporation at elevated temperatures. In a typical measurement, the reaction mixture of nanoplatelet growth was diluted 3 times the volume with a mixture of ODE and oleic acid (3:1) then placed in 1mm quartz optical cell equipped with a stirring bar. In order to prevent any adverse oxidation effects caused by the ambient atmosphere, the optical cells were filled and closed under inert atmosphere. Steady-state photoluminescence (PL) and time-resolved photoluminescence (TRPL)

measurements were carried out simultaneously for the samples measured in this study. Figure S5 shows a schematic for the PL/TRPL setup used for the measurements. The excitation laser employed was a frequency tripled (from 800 nm to 266 nm) ultrafast Ti:Sapphire laser (KM Labs Cascade cavity dumped oscillator) operating at 200 kHz with an approximate pulse width of 200 fs. For the steady-state PL measurements, PL spectra were collected slightly off normal incidence focused into a broadband 200 μm core-diameter optical fiber then into an Ocean Optics QE65000 spectrometer. For the TRPL measurements, a time correlated single photon counting (TCSPC) approach was used with PicoQuant - PicoHarp 300 TCSPC electronics and a 0.3 m Acton Research scanning monochromator to specify detection wavelength. The TRPL light was collected in a backscattering geometry. The sample cuvette was attached to a ceramic heater that was controlled by a calibrated RTD sensor and Lake Shore 340 temperature controller. Note: as the temperature of the samples was increased, the TRPL detection wavelength was controlled to match that of the peak PL emission collected from the Ocean Optics spectrometer. A white-light source with imaging optics was used to roughly find the optimal focal point for the PL/TRPL measurements. Once this was done, the white light source was turned off and further focusing adjustments were made to maximize the PL/TRPL signal with high resolution mechanical stages. During the entirety of PL/TRPL testing, samples were stirred with a micro-stir bar and stirring assembly (Ultrafast Systems) to ensure uniform temperature distribution and to help mitigate any photo-charging effects. The excitation laser was focused near the stirred area.

The X-ray diffraction (XRD) pattern of the CdTe platelets deposited on to the Si surface (cut 4 degrees off to eliminate the background) were obtained using a Siemens D500 powder diffractometer in the Bragg-Brentano geometry with CuK α radiation (see Fig. S4). Experimental lattice parameters were refined using the Materials Data, Inc., JADE 6.1 XRD Patterns processing software.

Photoluminescence Analysis.

In order to analyze the TRPL signals, PicoQuant FlouFit software was used to extract time constants and relative amplitudes of the TRPL signal. The time dependent TRPL signal intensity $I(t)$ can be modeled by the convolution of the TRPL instrument response function (IRF) and a multi exponential decay function, i.e.:

$$I(t) = \int_{-\infty}^t IRF(t') \sum_{i=1}^n \left(A_i e^{-\left(\frac{t-t'}{\tau_i}\right)} \right) dt'$$

The instrument response of our TRPL system was found to be approximately 100 ps; note: a Gaussian fit of the IRF is provided in Figure 3B of the main text. The amplitudes (A_i) and time constants (τ_i) of the biexponential fits are shown in the main text Figure 3C. In addition to the individual components of the emission dynamics, it is useful to calculate an average emission lifetime $\langle\tau\rangle$, which provides a weighted average of the biexponential decay. The average emission lifetime $\langle\tau\rangle$ can be calculated as $\langle\tau\rangle =$

$\frac{\sum_{i=1}^n A_i \tau_i^2}{\sum_{i=1}^n A_i \tau_i}$. The results of the average emission lifetime are displayed in Figure S7.

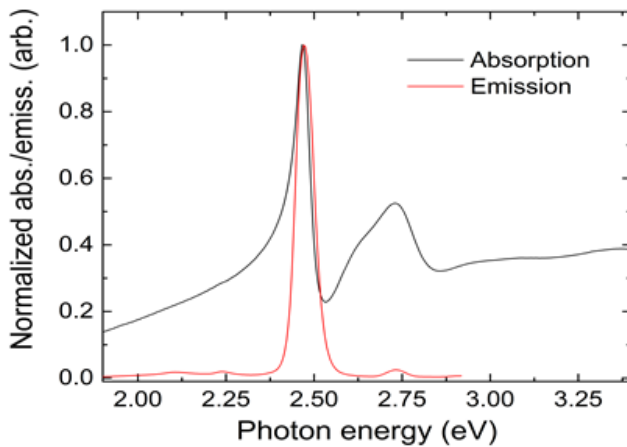


Figure S1. Absorption and emission spectra of a common NPL sample

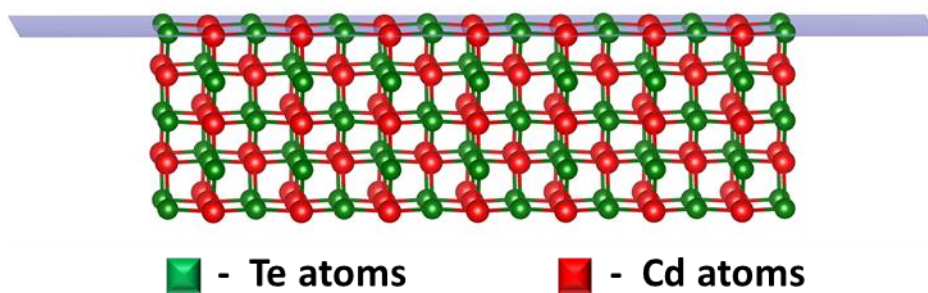


Figure S2. 3D Structural model of the CdTe platelets in [110] projection. Green atoms: Te; Red atoms: Cd.

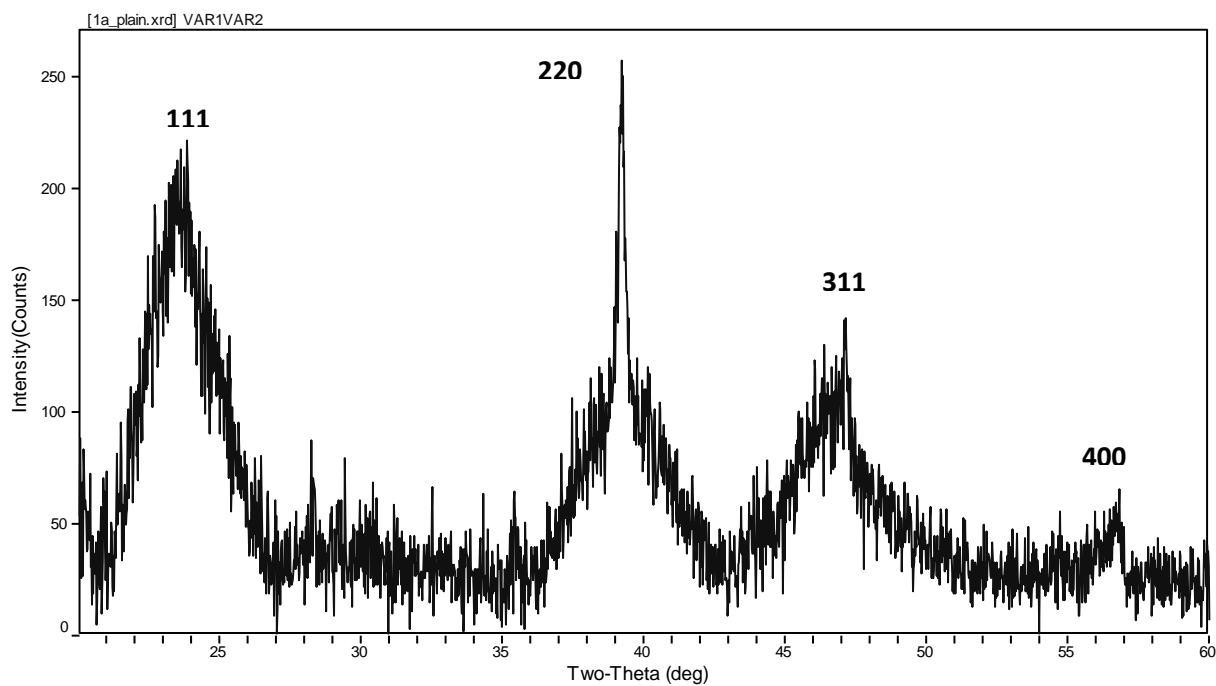


Figure S3. XRD scan for sample 41 indexed to the cubic phase (space group F-43m) with refined lattice parameter $a=6.473\pm 0.003$ Å. This value is in good agreement with the CdTe reference value of 6.48 Å

[PDF file #89-3053 from the ICDD database]. Narrow and high-intensity component in the 220 reflection indicates that the platelets basal surface is (220).

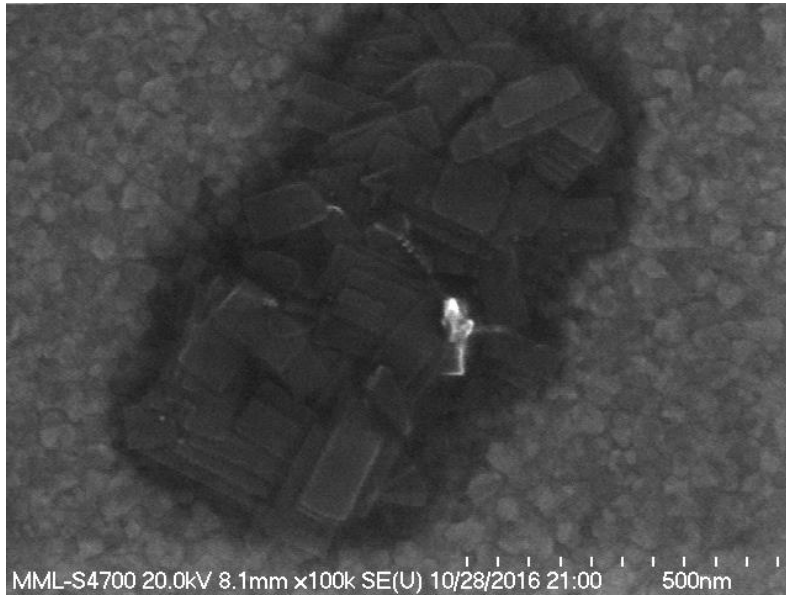


Figure S4. Plan-view SEM image of NPLs aggregates on Au-coated Si substrate

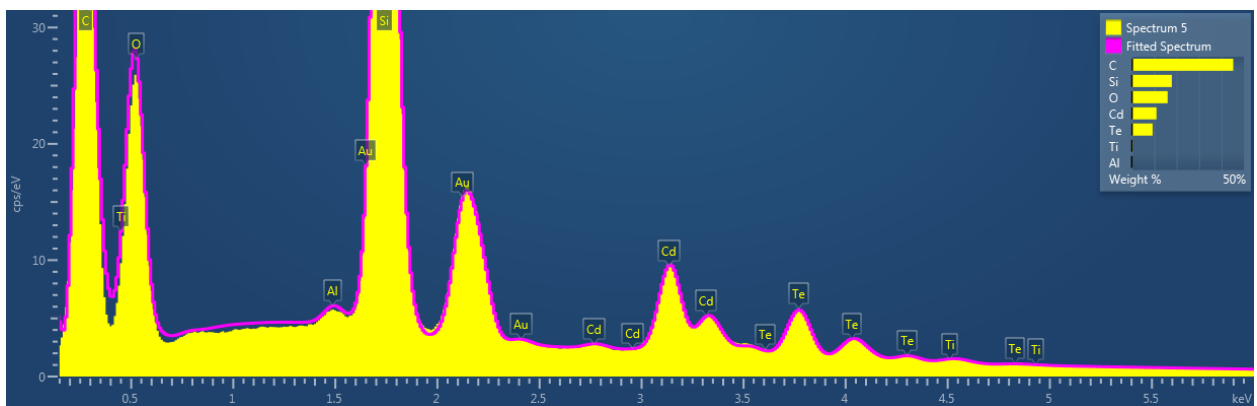


Fig. S5 EDS spectrum for the cadmium telluride NPLs with the composition of $\text{Cd}_{0.5+x}\text{Te}_{0.5-x}$, where $x=0.065(7)$

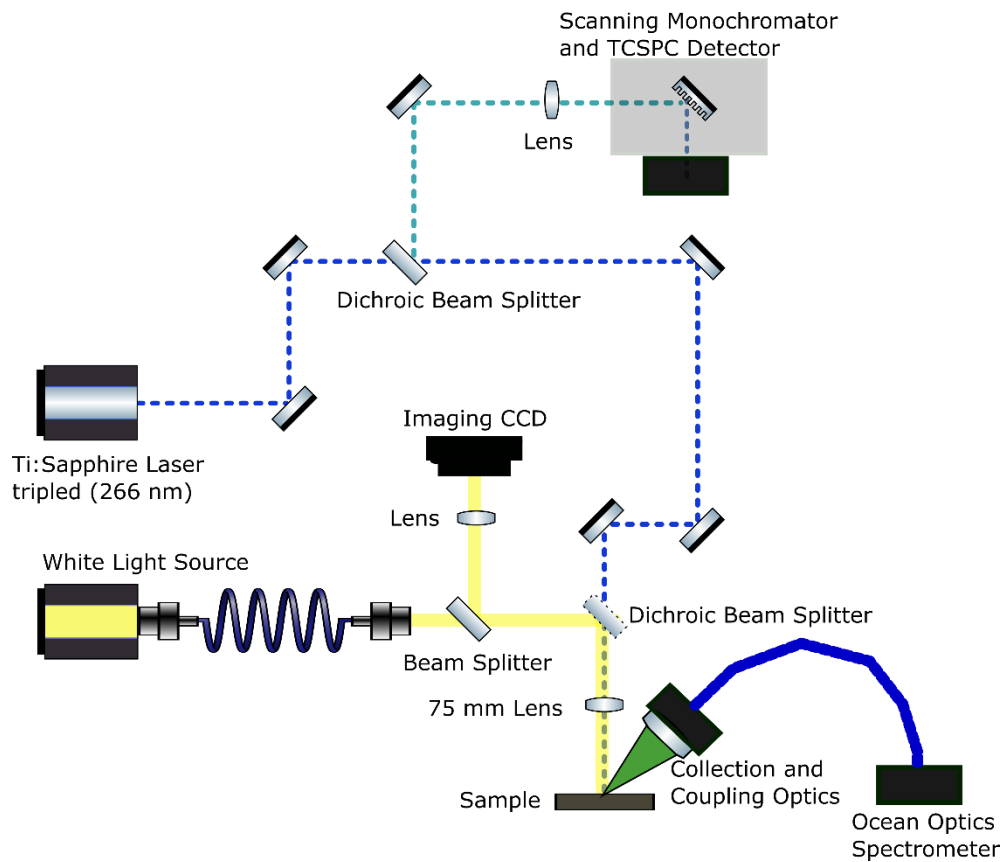


Figure S6: Experimental schematic for the simultaneous collection of PL and TRPL signals.

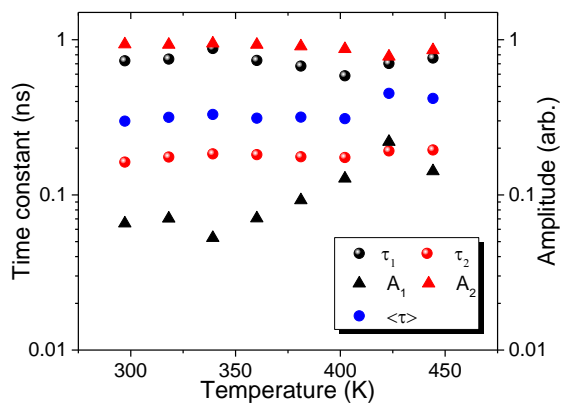


Figure S7: Emission lifetime components with calculated average lifetimes $\langle \tau \rangle$.

Additional PL data (showing non-complete recovery) with description of lifetimes and Varshini fittings.

Varshini fit was performed using a standard temperature dependence for bulk semiconductors, as it has been shown to be applicable to nanostructured materials (Chin, P.T.K.; Donegá, C.M.; van Bavel, S.S.; Meskers, S.C. J.; Sommerdijk, N.A.J.M.; Janssen R.A.J. *J. Am. Chem. Soc.*, **2007**, *129* (48), 14880–14886).

$$E_g = E_0 - \alpha \cdot T^2 / (T + \beta)$$

Where E_g is the band gap at a particular temperature, E_0 is the band gap at 0K, α is the temperature coefficient and β is Debye temperature.

Disclaimer: certain commercial equipment, instruments, or materials are identified in this paper in order to specify the experimental procedure adequately. Such identification is not intended to imply recommendation or endorsement by the National Institute of Standards and Technology.